HHS Public Access

Author manuscript

Neuroimage. Author manuscript; available in PMC 2018 March 01.

Published in final edited form as:

Neuroimage. 2017 March 01; 148: 219–229. doi:10.1016/j.neuroimage.2016.12.023.

Multimodal evaluation of the amygdala's functional connectivity

Rebecca Kerestes[a,*], **Henry W. Chase**[a], **Mary L. Phillips**[a], **Cecile D. Ladouceur**[a], and **Simon B. Eickhoff**[b,c]

[a]Department of Psychiatry, University of Pittsburgh School of Medicine, Pittsburgh, PA, USA

[b]Institute of Neuroscience and Medicine (INM-1), Research Center Jülich, Germany

[c]Institute of Clinical Neuroscience and Medical Psychology, Heinrich-Heine University Düsseldorf, Germany

Abstract

The amygdala is one of the most extensively studied human brain regions and undisputedly plays a central role in many psychiatric disorders. However, an outstanding question is whether connectivity of amygdala subregions, specifically the centromedial (CM), laterobasal (LB) and superficial (SF) nuclei, are modulated by brain state (i.e., task vs. rest). Here, using a multimodal approach, we directly compared meta-analytic connectivity modeling (MACM) and specific co-activation likelihood estimation (SCALE)-derived estimates of CM, LB and SF task-based co-activation to the functional connectivity of these nuclei as assessed by resting state fmri (rs-fmri). Finally, using a preexisting resting state functional connectivity-derived cortical parcellation, we examined both MACM and rs-fmri amygdala subregion connectivity with 17 large-scale networks, to explicitly address how the amygdala interacts with other large-scale neural networks. Analyses revealed strong differentiation of CM, LB and SF connectivity patterns with other brain regions, both in task-dependent and task-independent contexts. All three regions, however, showed convergent connectivity with the right ventrolateral prefrontal cortex (VLPFC) that was not driven by high base rate levels of activation. Similar patterns of connectivity across rs-fmri and MACM were observed for each subregion, suggesting a similar network architecture of amygdala connectivity with the rest of the brain across tasks and resting state for each subregion, that may be modified in the context of specific task demands. These findings support animal models that posit a parallel model of amygdala functioning, but importantly, also modify this position to suggest integrative processing in the amygdala.

[*]Corresponding author. Dr. Rebecca Kerestes, Western Psychiatric Institute and Clinic, Loeffler Building, 121 Meyran Avenue, Pittsburgh, PA, 15213; kerestesrv@upmc.edu.

Conflicts of interest

None of the authors declare any financial or other conflicts of interest that might have biased the work.
Dr. Phillips is a consultant for Roche.

Keywords

amygdala; meta-analytic connectivity modeling (MACM); specific co-activation likelihood estimation (SCALE); resting state; ventrolateral prefrontal cortex (VLPFC)

Introduction

In animals, a plethora of anatomical tracing (Adhikari et al. 2015; Carmichael and Price 1995; Cho et al. 2013; Fudge and Haber 2000; Ghashghaei et al. 2007; McDonald et al. 1996; Price et al. 1987), single cell recording (Faber et al. 2001; Mosher et al. 2010; Paré and Collins 2000) and lesion studies (Balleine et al. 2003; Cardinal et al. 2002; Killcross et al. 1997) have implicated the amygdala in emotional learning and memory processes, most notably, fear conditioning (LeDoux 2000; Maren 2001). However, over the last decade, evidence from human neuroimaging studies has lead to a broadened view of amygdala function that conceptualizes the region as a 'node' for detecting change in the environment. In line with this view, the amygdala's role is to evaluate the behavioral salience and motivational properties of sensory stimuli, as well as to subsequently generate appropriate emotional, autonomic and motor responses through connections with hypothalamic, thalamic and cortical brain regions (Sander et al. 2003). In the context of emotion regulation, connections between the amygdala and hypothalamic, thalamic and cortical brain regions are proposed to support rapid, often termed 'automatic' regulation of emotional behavior (Phelps and LeDoux 2005; Phillips et al. 2008).

Parcellation studies of the human amygdala have reliably shown that three major groups of nuclei may be distinguished on the basis of their histological features (Amunts et al. 2005), but also in-vivo based on structural (Solano-Castiella et al. 2011) and functional (Bzdok et al. 2013) connectivity patterns. Importantly, human connectivity-based parcellations of the amygdala show good concordance with cytoarchitectonic parcellations of the amygdala (Amunts et al. 2005). These nuclei, namely the centromedial (CM), laterobasal (LB) and superficial (SF) nuclei broadly resemble the microanatomy and connectivity of amygdala nuclei across mammalian species (McDonald 1998). Specifically, work done predominantly in monkeys and rodents have shown that the LB nuclei receive afferents from sensory cortical regions including the visual and auditory cortices and subcortical regions including the thalamus and hippocampus, but also dorsal and ventral medial parts of the PFC including the orbitofrontal cortex (OFC) (Adhikari et al. 2015; Amaral and Price 1984; Balleine and Killcross 2006; Cho et al. 2013; Ghashghaei et al. 2007; McDonald et al. 1996; Price 2006). These connections, which have also been observed in human neuroimaging studies (Bzdok et al. 2013), are consistent with a role of the LB nuclei in associative learning processes such as fear conditioning and reward-related learning (e.g., instrumental conditioning), and the integration of this information with self-relevant cognition (Bzdok et al. 2013).

The CM nuclei, which have classically been viewed as the major output region of the amygdaloid complex (McDonald 1998; Sah et al. 2003) are best known for being a generator of behavioral, autonomic and motor responses. Animal studies have shown dense connections between the CM nuclei and brainstem, hypothalamic and basal forebrain

regions (Fudge and Haber 2000; Ghashghaei et al. 2007; Sah et al. 2003). These findings have been corroborated by human neuroimaging studies and provide support for a role of the CM nuclei in motor behavior and response preparation in humans (Bzdok et al. 2013). Furthermore, influential animal models of amygdala functioning have proposed that the processing of emotional information and subsequent initiation of responses in the amygdala occurs in a serial (point-to-point) manner between LB and CM nuclei; that is, that pathways containing sensory information converge and integrate in LB nuclei and then proceed to the CM nuclei for the initiation of various responses (LeDoux 2000). Under the assumptions of this model, amygdala subregions would be expected to show a convergent pattern of connectivity with other brain regions. This serial model of amygdala processing has however, recently been challenged in favor of a parallel view of amygdala functioning (Balleine and Killcross 2006). Based on lesion studies in rodents, the parallel model proposes that the LB and CM nuclei work in parallel to mediate distinct aspects of incentive processing both in appetitive (i.e., reward) and aversive (i.e., punishment) contexts, and suggests that the LB and CM nuclei are independent nodes of key importance involved in emotional learning (Balleine 2005; Balleine and Killcross 2006). In contrast to a serial model of amygdala functioning, a parallel model of amygdala functioning would be expected to yield divergent patterns of CM and LB connectivity with other brain regions.

The SF nuclei, which are the least well characterized of the amygdala nuclei (McDonald 1998; Sah et al. 2003) are located adjacent to the LB nuclei and laterally to the CM nuclei (Price et al. 1987; Sah et al. 2003). SF nuclei have extensive bilateral connections with olfactory cortex, insular cortex, ventral striatum/nucleus accumbens and hippocampus/parahippocampal gyrus (Sah et al. 2003; Ubeda-Banon et al. 2007). These connections are consistent with the notion that the SF nuclei are involved in the detection of emotionally salient stimuli and the processing of socially relevant information including olfactory and emotional stimuli. In humans, an additional role of the SF nuclei in social cognition has been proposed, owing to strong connections between the SF nuclei and the anterior insula and inferior frontal gyrus (IFG) (Bzdok et al. 2013).

Recently, there has been increasing interest in understanding the functional organization of the human brain, in particular functional connectivity of widespread canonical networks during un-constrained (“resting state”) cognition (van den Heuvel and Hulshoff Pol 2010). An investigation of resting state amygdala connectivity that focused on the CM, LB and SF nuclei reported on distinct differences in amygdala connectivity with large scale networks that broadly resemble the aforementioned anatomical connections of the amygdala nuclei in rodents (Roy et al. 2009). Specifically, the LB nuclei were functionally connected with medial prefrontal cortical regions including the ventromedial PFC, superior frontal gyrus and the anterior cingulate cortex, and temporal regions including the hippocampus, parahippocampal gyrus and superior temporal gyrus. In contrast, the CM nuclei showed functional connectivity with striatal regions (nucleus accumbens extending to caudate), the thalamus, cerebellum and motor cortex. The SF nuclei were functionally connected with predominantly ‘limbic’ regions including the cingulate gyrus extending from dorsal ACC to subgenual ACC and the striatum as well as the ventromedial PFC.

A complimentary approach to studying resting state patterns of brain connectivity is provided by meta-analytic connectivity modeling (Fox et al. 2014; Laird et al. 2013). This approach to functional connectivity determines, using activation likelihood estimation (ALE), the co-occurrence of significant activations between every voxel in the brain and a 'seed region', across a database of neuroimaging experiments (Eickhoff et al. 2009). That is, MACM provides a complimentary method to understand the interactions of a given brain region within a co-activation framework, and provides a unifying account of functional connectivity (Cole et al. 2014; Eickhoff et al. 2015; Liu and Duyn 2013; Reid et al. 2016). In a previous MACM study (Bzdok et al. 2013), patterns of amygdala functional connectivity for the CM, LB and SF nuclei were broadly similar to the resting state fMRI (rs-fMRI) patterns of connectivity reported by Roy et al (2009). For example, in both studies, LB seeds showed connectivity with the ventromedial PFC. However, there were also some important differences. Most strikingly, was an apparent dissociation in connectivity of the amygdala nuclei with lateral compared to medial divisions of the PFC that was not observed in Roy et al (2009). Specifically, the CM and SF nuclei showed connectivity with bilateral ventrolateral prefrontal cortex (VLPFC); in contrast, the LB nuclei showed connectivity predominantly with bilateral medial PFC regions including the dorsal and ventral medial PFC (Bzdok et al. 2013). Furthermore, whereas the CM nuclei were connected to a region of the VLPFC proper, connectivity of the SF nuclei was with the more opercular region of the VLPFC, extending into the bilateral insula. Notably, in Roy et al (2009), functional connectivity with lateral prefrontal regions including the VLPFC, was largely absent for CM and LB nuclei and weak for the SF nuclei.

Taken together, the studies highlight outstanding questions regarding the functional connectivity of the amygdala. In particular, it is unclear if amygdala subregion connectivity with other brain regions including the VLPFC, changes as a function of different brain states (i.e. rest vs. task-based contexts), and if amygdala subregions are differentially modulated by brain state. The VLPFC, encompassing BA 45 (pars triangularis) and 47 (pars orbitalis) (Neubert et al. 2014; Petrides and Pandya 2002) is particularly relevant. First, it is a key neural region implicated in top-down voluntary regulation of emotional processing in the amygdala (Phillips et al. 2008), which, as shown by animal studies, is thought to be mediated by direct connections between the VLPFC and (predominantly LB) amygdala nuclei (Ghashghaei et al. 2007; see Ray and Zald 2012 for review). Second, in humans, altered amygdala-VLPFC connectivity has been found in several psychiatric disorders (Cha et al. 2016; Etkin et al. 2009) and is central to neurobiological models of Bipolar Disorder (BD) (Chase and Phillips 2016; Phillips and Swartz 2014). However, whether abnormalities in amygdala-VLPFC connectivity are subregion specific is less clear, as studies of amygdala connectivity typically examine the amygdala as a unitary structure, thus overlooking important distinct differences in connectivity between the CM, LB and SF amygdala nuclei.

Combining MACM and rs-fmri approaches provides the means to advance our understanding about amygdala brain functioning by identifying a core set of brain regions that are consistently functionally connected to the amygdala, independent of brain state. However, to date, no studies have directly compared amygdala connectivity patterns using these approaches. Addressing these outstanding questions about amygdala connectivity is also pertinent in the context of theories of human brain organization; that is, in

understanding how the amygdala interacts with other large-scale neural networks, and whether connectivity changes as a function of different brain states. Sophisticated models of brain connectivity that examine properties of information exchange across hierarchies of modularity in the brain have reported that the amygdala shows a high degree of embeddedness (Ye et al. 2015). Specifically, the amygdala shows high nodal efficiency and a slower decay rate of information exchange compared to other regions (Ye et al. 2015). Taking this view, the amygdala may show a varying degree of connectivity with several large-scale networks, as opposed to 'belonging' to a particular network (e.g., the default mode network; DMN, salience network; SN) that is influenced by changes in brain state. Systematically investigating and directly comparing task-dependent and task-independent connectivity of the amygdala is therefore a necessary step towards clarifying the role of the amygdala in the realm of brain network connectivity.

The primary aim of this study was to provide two conceptual replications by integrating the methods of Bzdok et al (2013) and Roy et al (2009), and extend upon this work by integrating a third modified MACM approach. This approach, called specific co-activation likelihood estimation (SCALE) accounts for base rate levels of activation for any given target region and is therefore less susceptible to the bias of particular regions that have a higher frequency of activation across studies (Langner et al. 2014). To test whether amygdala functioning more strongly reflects parallel (i.e., divergent) or serial (i.e., convergent) processing, shared variance of amygdala subregion time series needs to be modeled (Mumford et al. 2015). Our study, which sits apart from Bzdok et al (2013) and Roy et al (2009) by using an integrated approach, is therefore less biased toward detecting either divergent patterns of connectivity that occurs when time series are othogonalized (Roy et al. 2009) or convergent patterns of connectivity that are more likely to occur when machine learning-based approaches are used (Bzdok et al. 2013). A secondary aim was to explicitly test how the amygdala interacts with large-scale neural networks. Using a resting state functional connectivity-derived cortical parcellation (Yeo et al. 2011) we examined amygdala subregion connectivity with 17 large-scale networks (Yeo et al. 2011). In line with a parallel view of amygdala functioning (Balleine and Killcross 2006), our primary hypothesis was that the amygdala subregions would show distinct, independent patterns of functional connectivity. We also hypothesized that rs-fmri and MACM-derived patterns of functional connectivity would be different for the amygdala subregions, suggesting that context is critical, and that the amygdala subregions would be differentially context-dependent. Finally, in line with the idea of the amygdala showing a high degree of embeddedness, we predicted that all subregions of the amygdala would show positive and negative correlations with 17 large-scale neural networks, and that there would be subregion differences in connectivity with particular networks (e.g., DMN).

Methods

Volumes of interest (VOI)

The amygdala sub-region VOIs used for our analysis were derived from a histological definition of the amygdala using the SPM Anatomy toolbox (Eickhoff et al. 2006; Eickhoff et al. 2005; Figure 1). The 3 sub-divisions of the amygdala, namely the CM, LB and SF

nuclei, have been previously cytoarchitectonically mapped in ten human postmortem brains, 3D reconstructed and mapped to MNI (Montreal Neurological Institute) space (Amunts et al. 2005). The resulting “maximum probability map” (MPM) represents the most likely anatomical structure at each voxel of the reference space and hence provides a discrete representation of microanatomically defined areas in standard space. Importantly, these amygdala sub-regions have also been identified by connectivity-based parcellation of the human amygdala, showing spatial continuity and localization consistent with the cytoarchitectonically defined nuclei (Bzdok et al. 2013). The number of voxels in each of the three (bilateral) amygdala VOIs were as follows: CM nuclei = 68 voxels, LB nuclei = 688 voxels, SF nuclei = 138 voxels.

Data sources

BrainMap database—The MACM analysis used data derived from the BrainMap database (www.brainmap.org; Fox and Lancaster 2002; Laird et al. 2011). From this database, studies reporting fMRI and PET experiments in stereotaxic space from “normal mapping” studies in healthy participants, without interventions or group comparisons, were included. At the time of this study, the database contained approximately 67,620 peaks (coordinates) from 7,737 experiments reporting on 27,234 unique subjects.

Rockland sample—For the rs-fmri analysis, data were used from the Enhanced Nathan Kline Institute “Rockland” sample, available online via the International Neuroimaging Data sharing initiative (http://fcon_1000.projects.nitrc.org/indi/pro/nki.html). The sample consisted of 200 healthy subjects (76 M, 120 F), aged 20–50 (mean ± SD: 39.8 ± 15.06). This sample was chosen as it is a representative (adult lifetime) sample, and should thus provide results that can be assumed to be representative of the general population.

Functional connectivity analyses

Meta-analytic connectivity mapping (MACM)—Experiments were retrieved from the BrainMap database using procedures detailed in previous studies (see Bzdok et al. 2013 for detailed information). Briefly, experiments were identified in BrainMap that reported at least one focus of activation at or within the vicinity of the respective VOI. We included studies reporting fMRI and positron emission tomography (PET) experiments in stereotaxic space from “normal mapping” studies in healthy participants without interventions or group comparisons. The number of studies retrieved from the database for each of the three VOI’s were as follows: CM nuclei = 106 studies, LB nuclei = 313 studies, SF nuclei = 193 studies.

Following this, a coordinate-based meta-analysis was performed generating a brain-wide co-activation profile for each voxel in the VOI. The brain-wide co-activation pattern for each individual seed voxel was computed by activation likelihood estimation (Eickhoff et al. 2009; Turkeltaub et al. 2002) meta-analysis over the experiments that were associated with that particular voxel, to identify areas of converging activity across these experiments. The key idea behind ALE is to treat the foci reported in the associated experiments not as single points, but as centers for 3D Gaussian probability distributions that reflect the spatial uncertainty associated with neuroimaging results. In short, an ALE score for each voxel of the brain is computed that describes the co-activation probability of each particular location

in the brain with the current seed voxel. Significance of these co-activation probabilities is then computed by comparison with an analytical null distribution as described in Eickhoff et al (2012). The p values of each ALE score are then given by the proportion of equal or higher values under the null distribution. Following current recommendations (Eickhoff et al. 2016), ALE maps were thresholded at cluster-level $p<.05$, FWE corrected for multiple comparisons using a voxel-level height threshold of $p<.001$.

Specific co-activation likelihood estimation (SCALE)—In contrast to the conventional MACM algorithm, the modified MACM algorithm uses empirically derived voxel distributions that reflect the base rate of activation observed in a given voxel (Langner et al. 2014). This is thought to lead to more specific findings, by virtue of reducing over or underestimation of significant convergence. In order to best illustrate the distinction between MACM and SCALE, consider the example of the anterior insula. Given that this region is frequently activated across neuroimaging experiments, a high ALE score (reflecting co-activation with the amygdala) would be expected by the structure of the database. Comparing this against a global null-distribution, as done with MACM, would most likely give a significant finding in that region. In contrast, a region that does not show a high frequency of activation across neuroimaging experiments, but that is co-activated with the amygdala, would likely be associated with a medium ALE score. However, when comparing this against the null-distribution, this would likely yield a non-significant result. In SCALE, inference is permutation-based, whereby the probability of activation at each voxel is compared against a null-distribution. Here, the null-distribution reflects the inherent bias arising from the non-stationary likelihood of activation across the brain, by drawing random locations from the structure of the database and computing the ALE as for the real data. This process is repeated 2500 times to yield an empirical null-distribution of expected convergence at each voxel of the brain given the number of experiments activating the seed, having accounted for a priori activation at that voxel. Statistical inference (at a posterior probability of $P>.999$ for exceedance of the a priori likelihood) was then performed in order to identify those regions, where the convergence among the co-activations was above what could be explained by the structure of the BrainMap database. Here, due to the lack of a global null-distribution that is required to set a cluster-level FWE correction, the implementation of a cluster-level FWE correction is not possible.

It should be emphasized that both approaches (MACM and SCALE) have their own merits, and one is not necessarily better than the other. Rather, they are founded on different concepts of what significant co-activation means, and provide answers to different, but equally valid, neurobiological questions. Specifically, the conventional MACM approach is designed to yield co-activation patterns of a seed region, under the assumption of equal chances of spatial convergence for every grey matter voxel in the brain. The MACM approach therefore allows one to answer questions about what regions in *general*, show co-activation with a seed region.

In contrast, SCALE provides an increased level of specificity, by using an empirically-derived voxel distribution and is therefore comparing the pattern of co-activation for a given seed region, to what is expected. This approach allows one to answer questions about what brain regions *specifically* co-activate with a given seed region. In summary, SCALE is a

complimentary approach to the conventional MACM approach, and together, they provide a comprehensive picture of amygdala functional connectivity.

Resting state functional connectivity—We also delineated the task independent resting-state functional connectivity pattern of each of the CM, LB and SF nuclei using the NKI/Rockland sample described above. During the resting state scans subjects were instructed to keep their eyes closed and to think about nothing in particular but not to fall asleep (which was confirmed by post-scan debriefing). For each subject 260 resting state EPI images were acquired on a Siemens TimTrio 3T scanner using blood-oxygen-level-dependent (BOLD) contrast (gradient-echo EPI pulse sequence, TR = 2.5s, TE = 30ms, flip angle = 80°, in plane resolution = 3.0 × 3.0mm^2, 38 axial slices (3.0 mm thickness) covering the entire brain). The first four scans were excluded from further processing analysis using SPM8 to allow for magnet saturation. The remaining EPI images were first corrected for movement artifacts by affine registration using a two pass procedure in which the images were first aligned to the initial volumes and subsequently to the mean after the first pass. The obtained mean EPI of each subject was then spatially normalized to the MNI single subject template using the 'unified segmentation' approach (Ashburner and Friston 2005). The ensuing deformation was applied to the individual EPI volumes. To improve signal-to-noise ratio and compensate for residual anatomical variations images were smoothed with a 5-mm Full Width Half Maximum (FWHM) Gaussian kernel.

Based on previous evaluations (Satterthwaite et al. 2012), variance that was explained by the six motion parameters derived from the realignment step, their first derivative and their quadratic terms (i.e., a 24 parameter regression model), as well as the mean time-series' of WM/CSF (based on the SPM8 segmentation) was regressed out for each subject. After confound regression, the resulting residual timeseries were band pass filtered between 0.01 and 0.08Hz, as the majority of the power of the rsfMRI BOLD signal is present at these frequencies (Baria et al. 2013).

Subject-specific time courses were extracted from each of the amygdala VOIs (left and right CM, LB and SF nuclei) by computing the first eigenvariate of the time-series' of those voxels within the respective masks, whose grey matter probability was above the median across all voxels in the VOI. Linear (Pearson) correlation coefficients between the time series of the seed regions and all other gray matter voxels in the brain were computed to quantify rs-fMRI connectivity. Signal extraction for each of the left and right CM, LB and SF nuclei were done in separate models, resulting in 6 1st level models for each participant. These voxel-wise correlation coefficients were then transformed into Fisher's Z-scores and tested for consistency in a flexible factorial model across subjects. For 2nd level analyses, the main effect of connectivity for each of the left and right amygdala nuclei, as well as planned contrasts between the amygdala nuclei, were tested using the standard SPM8 implementations with the appropriate non-sphericity correction. Consistent with our MACM analyses, results were thresholded at cluster-level p<.05, FWE corrected for multiple comparisons using a voxel-level height threshold of p<.001.

Comparisons between rs-fmri, MACM and SCALE—Given the primary aim of our study, additional analyses were performed to investigate the similarity between: a) MACM

and rs-fmri and b) SCALE and rs-fmri. For these analyses, thresholded rs-fmri Z-score maps were masked using the thresholded maps from the MACM and SCALE analyses respectively. By doing so, inference was performed only within the regions identified as co-activated by a MACM analysis using the corresponding subregion as a seed. A cluster was reported as significant in Table 1 if a FWE-corrected voxelwise threshold of $p<0.05$ was reached (corrected for voxels within the MACM mask rather than the whole brain).

Network analysis

To explicitly examine how the amygdala interacts with other large-scale networks in the brain, we compared the analyses of MACM and rs-fmri amygdala connectivity with 17 large-scale networks, derived from a whole brain cortical parcellation of intrinsic network connectivity (Yeo et al. 2011). These included networks commonly examined in the literature: frontoparietal/control, dorsal attention, default mode, salience, limbic (cortical regions only), visual, temporoparietal and somatomotor networks. Detailed information including the regions contained in each network, along with the MNI coordinates of the clusters are reported in Yeo et al (2011) and Yeo et al (2015). For this analysis, we used the voxel-wise whole-brain rs-fmri statistical T map for each amygdala seed, from our rs-fmri analysis. We extracted the average T-value across voxels in each network. A Bonferrroni ($p<.05$ FWE) correction was then applied (minimum T statistic >4.9). For MACM, in order to render the maps comparable to rs-fmri, in spite of the fact that ALE scores scale with the number of experiments (Eickhoff et al., 2016), we normalized all MACM maps to a sum of one.

Results

MACM and SCALE co-activations

Individual MACM analyses for each of the amygdala subregions revealed that, despite some convergence of co-activation across all three subregions, the CM, LB and SF nuclei showed distinct patterns of co-activation with the rest of the brain, across studies in the BrainMap database (Table 1; Fig. 2). The CM nuclei showed co-activation with bilateral VLPFC and middle temporal lobe regions. The LB nuclei showed co-activation with more medial PFC regions including bilateral dorsal and ventral medial PFC, superior medial gyrus, and orbitofrontal gyrus as well as the right supplementary motor area (SMA). The SF nuclei showed co-activation with bilateral operculum extending into the insula, VLPFC, nucleus accumbens extending into the ventral putamen and the thalamus. Direct comparisons of the MACM connectivity maps largely revealed significant differences in co-activation between the subregions in regions identified by the initial subregion analysis described above (Table 1; **see** Supplementary Fig. 1). SCALE analyses yielded smaller, more circumscribed clusters of co-activation for each of the amygdala subregions. The spatial localization of the cluster peaks were, however, largely similar to MACM (Table 1; Fig. 2). For the CM seeds, co-activation with the right VLPFC remained; in contrast, co-activation with the left VLPFC did not. For the LB seeds, co-activation with dorsal and ventral medial PFC remained, although co-activation was stronger for the ventral medial PFC. For the SF seeds, co-activation with bilateral operculum and insula did not remain after base rate correcting,

however co-activation with the right VLPFC remained. Co-activation between the right SF seed and bilateral nucleus accumbens also remained.

Conjunction Analysis

A conjunction analysis of the MACM images for the left and right CM, LB and SF nuclei was conducted, to test for regions that were co-activated with all six amygdala subregions. This analysis revealed that all six amygdala subregions were co-activated with a cluster in the right VLPFC region of the IFG (specifically, pars triangularis corresponding to BA 45) and the bilateral fusiform gyrus. Importantly, the right VLPFC cluster remained when a conjunction analysis of the base rate corrected (i.e., SCALE) images was performed; however the bilateral fusiform gyrus did not.

To confirm a direct relationship between the right VLPFC and amygdala, we performed a MACM analysis (as above) using an empirically-derived ROI of the right VLPFC that was co-activated in our MACM and rs-fmri analyses (MNI coordinates: x= 52, y = 32, z = 6). These analyses, using the same statistical thresholding as described in our main analyses above, revealed that the right VLPFC is co-activated with the bilateral amygdala ($P<.05$, FWE, cluster-wise corrected; see Supplementary Fig. 3).

Additional MACM Analyses

We performed an additional MACM analysis, to ascertain if amygdala-right VLPFC co-activation was being driven by studies examining the processing and regulation of emotional information. To do this, we computed a contrast of all “emotion” vs. “non-emotion” studies in the BrainMap database. It is important to note that “emotion” comprises one of several behavioral domains (BD) into which studies are categorized for the purposes of classification in the BrainMap database. Studies within each BD can be further categorized into paradigm classes (PC) (e.g., passive viewing, emotion induction, emotion regulation). “Non-emotion” refers to all other BD’s including cognition, action, perception and interoception. For the purposes of this manuscript, here we focus on the contrast of all emotion studies vs. non-emotion studies. Statistical thresholding was kept consistent with our MACM analyses described above. These analyses revealed that for all amygdala subregions, co-activation in the right VLPFC was greater for emotion compared to non-emotion studies (Fig. 4a). In addition, all subregions showed co-activation in bilateral (albeit stronger for the left) ventral putamen and nucleus accumbens that was greater for emotion compared to non-emotion studies (see Supplementary Fig. 4). Interestingly, the inverse of this contrast (non-emotion > emotion) was associated with co-activation of the left VLPFC for the LB and SF seeds (Fig. 4b). Conjunction analyses demonstrating areas of common co-activation between emotion and non-emotion studies revealed co-activation with the bilateral fusiform gyrus for all amygdala sub-regions (Fig. 5). In addition, the LB seeds showed co-activation with the left VLPFC and bilateral ventromedial PFC (Fig. 5; left VLPFC not shown).

Resting state functional connectivity of the amygdala

The rs-fmri analysis revealed larger, more spatially wide-spread maps of functional connectivity for each amygdala subregion (Fig. 3; $p<.05$ FWE cluster-wise corrected).

Analysis of each amygdala seed region revealed that, in general, all subregions showed positive functional connectivity with the hippocampus/parahippocampal gyrus, caudate and putamen, anterior cingulate cortex (although stronger connectivity was seen between the SF seeds and the posterior cingulate cortex/precuneus), the insula, VLPFC, dorsal and ventral medial PFC (Fig. 3; also see Supplementary Table 1). In contrast, all amygdala subregions showed negative functional connectivity with the superior and inferior lateral occipital cortex, dorsolateral PFC (DLPFC) and orbitofrontal cortex. In addition, the SF seeds also showed negative functional connectivity with inferior temporal regions. We also performed pairwise contrasts between the left and right hemispheres for each amygdala subregion (see Supplementary Fig. 2). This analysis revealed differential connectivity in the ipsilateral hemisphere for each of the seeds. Specifically, the left CM, LB and SF seeds showed greater functional connectivity with left hemisphere regions compared to the right CM, LB and SF seeds, and vice versa. There were no regions of positive connectivity in one hemisphere that were negatively correlated in the contralateral hemisphere.

Comparisons between MACM, SCALE and rs-fmri

To test whether patterns of amygdala subregion rs-fmri connectivity were similar to MACM and SCALE, we examined rs-fmri positive and negative correlations with each amygdala subregion, masked by the MACM findings for the respective subregion (Table 1). The analyses showed that, in general, regions identified by the MACM and SCALE analyses also showed voxels with positive resting correlations with the corresponding amygdala subregion. For all amygdala subregions, co-activation and positive resting correlations were seen for bilateral hippocampus/parahippocampal gyrus, caudate and putamen, the insula, fusiform gyrus and the IFG. For SCALE the results were similar, although there were fewer clusters showing a positive correlation with rs-fmri, due to the smaller number of clusters identified by the SCALE analysis. Notably, co-activation with the right VLPFC, the bilateral dorsal and ventral medial PFC, and nucleus accumbens - regions that showed distinct co-activation with the CM, LB and SF seeds respectively - were all positively correlated with the respective seed during rest. There was however, an exception. Co-activation of the lateral occipital cortex that was identified by the MACM analysis for all amygdala subregions (but more strongly for the CM and LB seeds), showed negative connectivity with resting BOLD in the corresponding region.

Network Analysis

The results from this analysis are shown in Supplementary Fig. 5. As predicted, all amygdala subregions showed connectivity with 17 large-scale neural networks, during rest and task-based contexts. Significant positive correlations were seen with ventral somatomotor (left LB and SF nuclei), limbic cortical (LB nuclei), temporoparietal (left LB and SF nuclei) and default mode networks (SF nuclei) (all $p<.05$, FWE corrected). Significant negative correlations were seen with visual (CM nuclei) and frontoparietal/control networks (LB and SF nuclei). There were no statistically significant subregion differences in connectivity with individual networks. Qualitatively, however, subregion and hemispheric differences in connectivity emerged for the visual and default mode networks. Compared to the CM seeds, LB and SF seeds showed less negative connectivity with the visual networks. Similarly, the LB and SF seeds showed greater positive connectivity with

temporal lobe regions of the DMN (ICN 15), and hemispheric differences for all amygdala subregions emerged for the ventromedial PFC and posterior cingulate cortex (PCC) nodes of the DMN (ICN 17). For MACM, all amygdala subregions showed the greatest co-activation with ventral somatomotor, salience/ventral attention, temporoparietal and DMN networks. Qualitatively, when comparing MACM and rs-fmri, overall, networks that showed strong positive correlations with the amygdala during rest, also showed high co-activation with the amygdala during tasks. There were, however, some differences. The most notable was for visual networks. Here, all amygdala subregions showed negative rs-fmri connectivity with visual networks; in contrast all subregions showed positive task based co-activation with visual networks (Supplementary Fig. 5). This is in line with our rs-fmri and MACM findings (see Results). In addition, whereas all amygdala sub-regions showed negative rs-fmri connectivity with a dorsal attention network (ICN 5), all subregions showed positive task-based co-activation with this network.

Discussion

In the present study, we employed a multimodal approach to examine and compare rs-fmri and task-dependent amygdala subregion functional connectivity, to address outstanding questions about how the amygdala interacts with other brain regions, and more broadly, large-scale networks. Our results, which are in line with the work of Bzdok et al (2013) and Roy et al (2009), provide convergent evidence of a parallel model of amygdala functioning. This was evidenced by strong differentiation of CM, LB and SF connectivity with other brain regions, both in task-dependent and task-independent contexts. Importantly however, our results also modify this position, by showing evidence of convergence between the CM, LB and SF nuclei, in the right VLPFC. Finally our observation of similar rs-fmri and task-dependent functional connectivity profiles for each amygdala subregion suggests a similar network architecture of amygdala connectivity with the rest of the brain across both tasks and resting state, that may be modified in the context of specific task demands. Our finding of amygdala-right VLPFC co-activation that was greater in the context of emotion (vs. non-emotion) studies provides empirical support for this proposition.

Subregion differences in amygdala connectivity: Replication of previous findings and comparisons with other studies

In line with our hypothesis, we found strong differentiation of CM, LB and SF co-activation profiles with other brain regions. Whereas the CM nuclei were co-activated with bilateral VLPFC (albeit stronger for the right), the LB nuclei were co-activated with more medial regions of the PFC including the bilateral dorsal and ventral medial PFC. Finally, the SF nuclei showed co-activation with the bilateral operculum extending into the insula and the nucleus accumbens. These findings largely replicate the work of Bzdok et al (2013), who also showed strong task-based differentiation of amygdala nuclei functional connectivity, particularly with medial and lateral parts of the PFC. Our results also largely support the findings of Roy et al (2009) who showed distinct resting-state functional connectivity patterns of amygdala subregions. Functional specialization of amygdala subregions has been shown to emerge during development, with relatively undifferentiated CM and LB resting-state connectivity characteristic of childhood, becoming increasingly differentiated by early

adulthood (Qin et al. 2012). Functional specialization of amygdala subregions has also been demonstrated in previous investigations of amygdala connectivity that have used data-driven rs-fmri connectivity-based (Mishra et al. 2014), as well as probabilistic tractography-based (Bach et al. 2011) parcellations of the human amygdala. Whilst direct comparisons are not possible, these methods yield similar brain-wide connectivity patterns for each of the amygdala subregions to those reported in the present manuscript.

Our findings also broadly map on to known anatomical connections of the amygdala in monkeys, cats and rodents (Ghashghaei et al. 2007; McDonald 1998; Musil and Olson 1988). Work done predominantly in rodents and monkeys has shown that the LB nuclei are a major target of afferent projections from medial divisions of the PFC including the ventromedial PFC, subgenual ACC and OFC (Carmichael and Price 1995; Ghashghaei et al. 2007; McDonald 1998; Stefanacci and Amaral 2002). In turn, efferent projections from the LB nuclei target medial PFC regions, with the heaviest projections to the posterior OFC, anterior insula and anterior cingulate cortex (mainly subgenual ACC but also anterior mid cingulate cortex; aMCC) (Öngur and Price 2000). These brain regions develop early and cytoarchitecturally lack a well-defined granular cortical layer IV (i.e., they are agranular and dysgranular) (Carmichael and Price 1994). In humans, these connections are thought to underlie top-down control of emotion (Ochsner and Gross 2005; Phan et al. 2002; Phillips et al. 2008). The CM and SF nuclei also receive input from the medial PFC, although to a lesser extent (Stefanacci and Amaral 2002), consistent with our observations. In line with (Bzdok et al. 2013), all amygdala regions showed connectivity with the ventral striatum, however this was greater for the SF nuclei (see Supplementary material Figure 1). These findings provide support for parallel, independent processing in the amygdala and speak to the importance of examining amygdala subregions separately rather than treating the amygdala as a unitary structure, to better understand amygdala functional specialization.

Amygdala-Right VLPFC connectivity

Perhaps the most striking finding of the present study was convergent co-activation and rs-fmri functional connectivity between all amygdala subregions and the right VLPFC, specifically in pars triangularis (BA 45). This was confirmed by a formal conjunction analysis (see Results). Importantly, whilst we also observed co-activation between all amygdala subregions and the bilateral fusiform gyrus, this effect was accounted for by high rates of activation, evidenced by a lack of this region in our conjunction analysis of SCALE images. In contrast, amygdala co-activation with the right VLPFC was not driven by base rate levels of activation in the right VLPFC (Table 1). As stated previously, an earlier MACM investigation also reported amygdala connectivity with the VLPFC, however a resting state investigation of amygdala connectivity showed largely absent connectivity between these two regions (Roy et al. 2009). This is the first study to demonstrate convergent activity between the CM, LB and SF amygdala nuclei in the right VLPFC using an integrated approach, and provides support for rodent studies that suggest an integrative/serial model of amygdala functioning. Interestingly, this region of the IFG is one whose rodent/human homology is not well understood. Based on studies predominantly in monkeys, the VLPFC component of the IFG comprises BA 45 (pars triangularis) and 47 (pars orbitalis) (Neubert et al. 2014; Petrides and Pandya 2002). Reasonable homology

between the human and monkey VLPFC has been found, with posterior lateral area 12 in the macaque and rhesus monkeys showing architectonic characteristics similar to BA 47 in humans (Ghashghaei et al. 2007; Neubert et al. 2014; Petrides and Pandya 2002). Lateral regions of the PFC including the VLPFC but also the DLPFC have sparse projections to the amygdala in comparison to medial PFC regions (Ghashghaei et al. 2007; Stefanacci and Amaral 2002). Lateral PFC regions develop late and are characterized by a well-defined granular cortical layer IV (Barbas and Pandya 1989).

Animal studies have shown that, in contrast to the DLPFC, the VLPFC receives modest projections from the LB nuclei, but has dense projections to the amygdala (Ghashghaei et al. 2007). This suggests that the VLPFC has a direct role in emotion regulatory processes. Our results provide empirical support for this. Firstly, our findings confirmed a direct relationship between the amygdala and right VLPFC. Secondly, we showed that although amygdala-right VLPFC co-activation appeared to be insensitive to brain state (i.e. task vs. rest), pronounced differences emerged when comparing emotion to non-emotion studies, where amygdala-right VLPFC co-activation was driven by studies that employed emotional processing paradigms. Taken together, our findings suggest that there is a common network architecture of amygdala connectivity that is preserved across brain states, but is modified as necessary, in the context of specific task demands (see Cole et al. 2014; Reid et al. 2016). Finally, we also found laterality effects in the VLPFC in the context of emotion vs. non-studies. Specifically, the right and left VLPFC were co-activated to a greater extent by emotion and non-emotion studies, respectively. Both the left and right VLPFC play a critical role in voluntary emotion regulation subprocesses including cognitive control processes such as cognitive reappraisal (Buhle et al. 2013; Vincent et al. 2008). There is, however, some evidence to show that right lateral regions of the PFC, especially the VLPFC, are more involved in the selection and/or inhibition of various kinds of responses, particularly when cognitive alterations of subjective emotion are involved (e.g., coping with the subjective feeling of being distracted) (Dolcos and McCarthy 2006; Iordan et al. 2013; Ochsner et al. 2002). Although it is beyond the scope of this paper to explicitly test this, it is possible that recruitment of the right VLPFC and/or the magnitude of amygdala-right VLPFC co-activation may depend on the type of emotion paradigm being used (e.g., fear processing vs. cognitive reappraisal of emotion). These remain plausible hypotheses for future testing.

Our findings also have implications for understanding altered functioning of the VLPFC and amygdala in psychiatric disorders. Indeed, altered activation and connectivity of the VLPFC is proposed to play a central role in the pathophysiology of Bipolar Disorder (BD). For example, reduced VLPFC activation and concomitant elevated amygdala activation during emotion processing tasks has been consistently reported in BD (Phillips and Swartz 2014). Furthermore, BD patients exhibit abnormally elevated functional connectivity between the amygdala and VLPFC during both rest and emotional processing (Chase and Phillips 2016). Elevated amygdala-VLPFC connectivity has also been reported in unaffected offspring at risk for BD (Manelis et al. 2015) and unaffected first-degree relatives (Dima et al. 2016). However, directionality of this effect has not been consistent, with some evidence of reduced right VLPFC-amygdala connectivity in healthy offspring of BD parents (Ladouceur et al. 2013). Together, these data point towards an altered amygdala-VLPFC relationship as a possible endophenotype of bipolar disorder (Chase and Phillips 2016). Our present findings

provide further insights into the nature of this relationship. First, the VLPFC appears to show relatively consistent connectivity with each of the three amygdala subregions and across modality, confirming a central role for this region in regulating the amygdala as a whole. Second, the relationship of the ventromedial PFC with the amygdala is relatively specific for the LB subregion, implying that the regular observations of altered medial PFC-amygdala connectivity in BD (Chase and Phillips 2016) relate to the LB amygdala rather than the other subregions (but see Liu et al 2013). Overall, these findings point to the importance of examining amygdala subregions separately to delineate, with greater specificity, the nature of amygdala-VLPFC alterations in psychiatric disorders.

Amygdala connectivity with large-scale neural networks

An outstanding question in the literature is how the amygdala interacts with other large-scale neural networks. Mainly informed by rs-fmri studies, the amygdala is often considered a part of the DMN, mainly owing to connections (both anatomical as discussed above, but also functional connections) between the LB nuclei and the medial PFC (Andrews-Hanna et al. 2010; Buckner et al. 2008). The amygdala has also been suggested to be a part of the SN (Seeley et al. 2007), playing a central role in salience detection and emotional processing, and due to its connectional organization with key regions implicated in social cognition, is considered a hub region, anchoring large-scale networks that play a central role in social behaviors (Bickart et al. 2014). Most undisputedly, is the amygdala's involvement in an emotion regulation network where it is involved in detecting the salience of environmental stimuli and the generation of affective arousal (Phillips et al. 2008). Connections between the amygdala and nodes in these neural networks are most often attributed to the LB nuclei. Here, we explicitly examined amygdala subregion connectivity with 17 large-scale neural networks during rest and task-based contexts. These networks broadly correspond to major networks discussed in the literature including the aforementioned DMN and salience networks. Our results provide direct evidence for our a priori hypothesis; that is that the amygdala is a highly embedded region, showing a diffuse pattern of integration with particular large-scale neural networks, during rest and task-based contexts. However, when interpreting the findings, we recognize the importance of distinguishing the statistically significant results from the more qualitative findings. Whereas the former can be used to directly support our a priori hypothesis, the latter can merely be used to provoke future research hypotheses about amygdala connectivity. Specifically, significant positive correlations were seen with networks including cortical limbic regions, ventral somatomotor regions, as well as nodes in the salience and temporoparietal networks. From an evolutionary point of view, connectivity with these networks, particularly limbic cortical regions that develop earlier evolutionarily, would allow for a high degree of integration of emotional information, which, in turn, would require diffuse and efficient access to other brain networks. Qualitatively, whilst distinct subregion differences were not observed for many networks, the LB and SF seeds showed greater connectivity with temporal lobe regions of the DMN compared to CM seeds. In addition, hemispheric differences were seen for the ventromedial PFC and posterior cingulate cortex nodes of the DMN, with left hemisphere amygdala subregions showing greater connectivity than the corresponding right hemisphere subregion. These results may suggest that LB and SF nuclei are more strongly connected to hub regions of the DMN compared to the CM nuclei, which, instead, show stronger

connectivity with more primitive motor and visual regions, consistent with animal studies. However this discussion is speculative and these ideas remain plausible hypotheses for future testing in both healthy and psychiatric populations. In summary, our results suggest that the amygdala exhibits both diffuse connectivity with particular large-scale neural networks, allowing for efficient communication across the brain and integration of information, as well as specific connectivity with core regions including the bilateral fusiform gyrus and right VLPFC. It is plausible that the fusiform gyrus and right VLPFC may facilitate connectivity between the amygdala and particular neural networks, but this remains to be tested in future work.

There are some limitations of the present study. Firstly, the small size of our VOI and resolution of imaging studies within the BrainMap database makes it difficult to distinguish the amygdala from other nearby regions. However, our VOI is based on well-defined cytoarchitectonic probability maps of the human amygdala that have been previously published (Amunts et al. 2005) and used in a previous MACM investigation of amygdala co-activation (Bzdok et al. 2013). Furthermore, the ALE method employed in the present study, is based on activation peaks of functional clusters as opposed to the 3D shape of the BOLD signal, and is therefore not affected by spatial smoothing that is applied in neuroimaging studies. Good concordance is also seen between the neuroimaging data-derived and cytoarchitectonic-derived subregions of the amygdala (see Bzdok et al. 2013) and we are therefore confident in the spatial resolution of the VOI in the present study. In addition, whilst sex was included as a covariate of no interest in the rs-fmri analyses, we did not have sufficient information (e.g., menstrual cycle phase, hormone levels) to thoroughly test for sexual dimorphism effects in our rs-fmri analyses. Indeed, sex differences in rs-fmri amygdala connectivity with brain regions including the IFG as well as different regulatory effects of cortisol on amygdala connectivity have been reported in healthy adults (Kogler et al. 2016). Finally, like many previous studies, we used conventional methods for our rs-fmri connectivity analysis. These are based on stationary correlations between brain regions and do not take into account potential non-stationary (dynamic) functional connectivity patterns (Chang and Glover 2010), that may actually be dominated by brief instances of spontaneous co-activation of brain regions (Liu and Duyn 2013). These findings, along with other studies (Karahanoglu and Van De Ville 2015; Liu et al. 2013) provide further support for co-activation being a unifying account of functional connectivity, and will pave the way for future studies examining dynamic amygdala functional connectivity with the rest of the brain.

In summary, we employed a multi-modal approach to identify brain regions functionally interacting with the CM, LB and SF amygdala nuclei during rest and task-based contexts, to ascertain if amygdala connectivity was influenced by brain state, and if this differed across amygdala subregions. We extended upon this further to examine diffuse amygdala connectivity with 17 large-scale neural networks. Our primary results provide support for a parallel model of amygdala functioning, with distinct subregion co-activation and connectivity patterns likely to reflect the functional specialization of this region. However, we also provide evidence of convergent processing between the CM, LB and SF amygdala nuclei in the right VLPFC. We propose that the right VLPFC is a core region consistently interacting with the amygdala, that connectivity between these two regions in highly

selective, and that connectivity between them may change as a function of task demands. Our findings also provide support for the idea that the amygdala is a highly embedded region that interacts with many large-scale brain networks. Future studies examining amygdala-right VLPFC temporal dynamic functional connectivity will provide valuable insight into the nature of amygdala connectivity with the right VLPFC and how such connectivity varies across both individuals and brain states.

Supplementary Material

Refer to Web version on PubMed Central for supplementary material.

Acknowledgments

Funding

Funding: This study was supported by the Deutsche Forschungsgemeinschaft (DFG, EI 816/4-1, LA 3071/3-1; EI 816/6-1.), the National Institute of Mental Health R01 Grants (MH074457; PI: Fox), (MH099007; PI: Ladouceur) and (MH100041-03; PI: Phillips), the Helmholtz Portfolio Theme "Supercomputing and Modeling for the Human Brain" and the European Union Seventh Framework Programme (FP7/2007–2013) under grant agreement no. 604102). Dr. Phillips is also funded by the Pittsburgh Foundation-Emmerling Endowed Chair in Psychotic Disorders.

References

Adhikari A, Lerner TN, Finkelstein J, Pak S, Jennings JH, Davidson TJ, Ferenczi E, Gunaydin LA, Mirzabekov JJ, Ye L, Kim SY, Lei A, Deisseroth K. Basomedial amygdala mediates top-down control of anxiety and fear. Nature. 2015; 527:179–185. [PubMed: 26536109]

Amaral DG, Price JL. Amygdalo-cortical projections in the monkey (Macaca fascicularis). J Comp Neurol. 1984; 230:465–496. [PubMed: 6520247]

Amunts K, Kedo O, Kindler M, Pieperhoff P, Mohlberg H, Shah NJ, Habel U, Schneider F, Zilles K. Cytoarchitectonic mapping of the human amygdala, hippocampal region and entorhinal cortex: intersubject variability and probability maps. Anat Embryol (Berl). 2005; 210:343–352. [PubMed: 16208455]

Andrews-Hanna JR, Reidler JS, Sepulcre J, Poulin R, Buckner RL. Functional-anatomic fractionation of the brain's default network. Neuron. 2010; 65:550–562. [PubMed: 20188659]

Ashburner J, Friston KJ. Unified segmentation. Neuroimage. 2005; 26:839–851. [PubMed: 15955494]

Bach DR, Behrens TE, Garrido L, Weiskopf N, Dolan RJ. Deep and superficial amygdala nuclei projections revealed in vivo by probabilistic tractography. J Neurosci. 2011; 31:618–623. [PubMed: 21228170]

Balleine BW. Neural bases of food-seeking: affect, arousal and reward in corticostriatolimbic circuits. Physiol Behav. 2005; 86:717–730. [PubMed: 16257019]

Balleine BW, Killcross AS, Dickinson A. The effect of lesions of the basolateral amygdala on instrumental conditioning. J Neurosci. 2003; 23:666–675. [PubMed: 12533626]

Balleine BW, Killcross S. Parallel incentive processing: an integrated view of amygdala function. Trends Neurosci. 2006; 29:272–279. [PubMed: 16545468]

Barbas H, Pandya DN. Architecture and intrinsic connections of the prefrontal cortex in the rhesus monkey. J Comp Neurol. 1989; 286:353–375. [PubMed: 2768563]

Baria AT, Mansour A, Huang L, Baliki MN, Cecchi GA, Mesulam MM, Apkarian AV. Linking human brain local activity fluctuations to structural and functional network architectures. Neuroimage. 2013; 73:144–155. [PubMed: 23396160]

Bickart KC, Dickerson BC, Barrett LF. The amygdala as a hub in brain networks that support social life. Neuropsychologia. 2014; 63:235–248. [PubMed: 25152530]

Buckner RL, Andrews-Hanna JR, Schacter DL. The brain's default network: anatomy, function, and relevance to disease. Ann N Y Acad Sci. 2008; 1124:1–38. [PubMed: 18400922]

Buhle JT, Silvers JA, Wager TD, Lopez R, Onyemekwu C, Kober H, Weber J, Ochsner KN. Cognitive Reappraisal of Emotion: A Meta-Analysis of Human Neuroimaging Studies. Cereb Cortex. 2013

Bzdok D, Laird AR, Zilles K, Fox PT, Eickhoff SB. An investigation of the structural, connectional, and functional subspecialization in the human amygdala. Hum Brain Mapp. 2013; 34:3247–3266. [PubMed: 22806915]

Cardinal RN, Parkinson JA, Hall J, Everitt BJ. Emotion and motivation: the role of the amygdala, ventral striatum, and prefrontal cortex. Neurosci Biobehav Rev. 2002; 26:321–352. [PubMed: 12034134]

Carmichael ST, Price JL. Architectonic subdivision of the orbital and medial prefrontal cortex in the macaque monkey. J Comp Neurol. 1994; 346:366–402. [PubMed: 7527805]

Carmichael ST, Price JL. Limbic connections of the orbital and medial prefrontal cortex in macaque monkeys. J Comp Neurol. 1995; 363:615–641. [PubMed: 8847421]

Cha J, DeDora D, Nedic S, Ide J, Greenberg T, Hajcak G, Mujica-Parodi LR. Clinically Anxious Individuals Show Disrupted Feedback between Inferior Frontal Gyrus and Prefrontal-Limbic Control Circuit. J Neurosci. 2016; 36:4708–4718. [PubMed: 27122030]

Chang C, Glover GH. Time-frequency dynamics of resting-state brain connectivity measured with fMRI. Neuroimage. 2010; 50:81–98. [PubMed: 20006716]

Chase HW, Phillips ML. Elucidating Neural Network Functional Connectivity Abnormalities in Bipolar Disorder: Toward a Harmonized Methodological Approach. Biological Pychiatry: CNNI. 2016; 1:288–298.

Cho YT, Ernst M, Fudge JL. Cortico-amygdala-striatal circuits are organized as hierarchical subsystems through the primate amygdala. J Neurosci. 2013; 33:14017–14030. [PubMed: 23986238]

Cole MW, Bassett DS, Power JD, Braver TS, Petersen SE. Intrinsic and task-evoked network architectures of the human brain. Neuron. 2014; 83:238–251. [PubMed: 24991964]

Dima D, Roberts RE, Frangou S. Connectomic markers of disease expression, genetic risk and resilience in bipolar disorder. Transl Psychiatry. 2016; 6:e706. [PubMed: 26731443]

Dolcos F, McCarthy G. Brain systems mediating cognitive interference by emotional distraction. J Neurosci. 2006; 26:2072–2079. [PubMed: 16481440]

Eickhoff SB, Bzdok D, Laird AR, Kurth F, Fox PT. Activation likelihood estimation meta-analysis revisited. Neuroimage. 2012; 59:2349–2361. [PubMed: 21963913]

Eickhoff SB, Heim S, Zilles K, Amunts K. Testing anatomically specified hypotheses in functional imaging using cytoarchitectonic maps. Neuroimage. 2006; 32:570–582. [PubMed: 16781166]

Eickhoff SB, Laird AR, Grefkes C, Wang LE, Zilles K, Fox PT. Coordinate-based activation likelihood estimation meta-analysis of neuroimaging data: a random-effects approach based on empirical estimates of spatial uncertainty. Hum Brain Mapp. 2009; 30:2907–2926. [PubMed: 19172646]

Eickhoff SB, Nichols TE, Laird AR, Hoffstaedter F, Amunts K, Fox PT, Bzdok D, Eickhoff CR. Behavior, sensitivity, and power of activation likelihood estimation characterized by massive empirical simulation. Neuroimage. 2016; 137:70–85. [PubMed: 27179606]

Eickhoff SB, Stephan KE, Mohlberg H, Grefkes C, Fink GR, Amunts K, Zilles K. A new SPM toolbox for combining probabilistic cytoarchitectonic maps and functional imaging data. Neuroimage. 2005; 25:1325–1335. [PubMed: 15850749]

Eickhoff SB, Thirion B, Varoquaux G, Bzdok D. Connectivity-based parcellation: Critique and implications. Hum Brain Mapp. 2015; 36:4771–4792. [PubMed: 26409749]

Etkin A, Prater KE, Schatzberg AF, Menon V, Greicius MD. Disrupted amygdalar subregion functional connectivity and evidence of a compensatory network in generalized anxiety disorder. Arch Gen Psychiatry. 2009; 66:1361–1372. [PubMed: 19996041]

Faber ES, Callister RJ, Sah P. Morphological and electrophysiological properties of principal neurons in the rat lateral amygdala in vitro. J Neurophysiol. 2001; 85:714–723. [PubMed: 11160506]

Fox PT, Lancaster JL. Opinion: Mapping context and content: the BrainMap model. Nat Rev Neurosci. 2002; 3:319–321. [PubMed: 11967563]

Fox PT, Lancaster JL, Laird AR, Eickhoff SB. Meta-analysis in human neuroimaging: computational modeling of large-scale databases. Annu Rev Neurosci. 2014; 37:409–434. [PubMed: 25032500]

Fudge JL, Haber SN. The central nucleus of the amygdala projection to dopamine subpopulations in primates. Neuroscience. 2000; 97:479–494. [PubMed: 10828531]

Ghashghaei HT, Hilgetag CC, Barbas H. Sequence of information processing for emotions based on the anatomic dialogue between prefrontal cortex and amygdala. Neuroimage. 2007; 34:905–923. [PubMed: 17126037]

Iordan AD, Dolcos S, Dolcos F. Neural signatures of the response to emotional distraction: a review of evidence from brain imaging investigations. Front Hum Neurosci. 2013; 7:200. [PubMed: 23761741]

Karahanoglu FI, Van De Ville D. Transient brain activity disentangles fMRI resting-state dynamics in terms of spatially and temporally overlapping networks. Nat Commun. 2015; 6:7751. [PubMed: 26178017]

Killcross S, Robbins TW, Everitt BJ. Different types of fear-conditioned behaviour mediated by separate nuclei within amygdala. Nature. 1997; 388:377–380. [PubMed: 9237754]

Kogler L, Muller VI, Seidel EM, Boubela R, Kalcher K, Moser E, Habel U, Gur RC, Eickhoff SB, Derntl B. Sex differences in the functional connectivity of the amygdalae in association with cortisol. Neuroimage. 2016; 134:410–423. [PubMed: 27039701]

Ladouceur CD, Diwadkar VA, White R, Bass J, Birmaher B, Axelson DA, Phillips ML. Fronto-limbic function in unaffected offspring at familial risk for bipolar disorder during an emotional working memory paradigm. Dev Cogn Neurosci. 2013; 5:185–196. [PubMed: 23590840]

Laird AR, Eickhoff SB, Fox PM, Uecker AM, Ray KL, Saenz JJ Jr, McKay DR, Bzdok D, Laird RW, Robinson JL, Turner JA, Turkeltaub PE, Lancaster JL, Fox PT. The BrainMap strategy for standardization, sharing, and meta-analysis of neuroimaging data. BMC Res Notes. 2011; 4:349. [PubMed: 21906305]

Laird AR, Eickhoff SB, Rottschy C, Bzdok D, Ray KL, Fox PT. Networks of task co-activations. Neuroimage. 2013; 80:505–514. [PubMed: 23631994]

Langner R, Rottschy C, Laird AR, Fox PT, Eickhoff SB. Meta-analytic connectivity modeling revisited: controlling for activation base rates. Neuroimage. 2014; 99:559–570. [PubMed: 24945668]

LeDoux JE. Emotion circuits in the brain. Annu Rev Neurosci. 2000; 23:155–184. [PubMed: 10845062]

Liu X, Chang C, Duyn JH. Decomposition of spontaneous brain activity into distinct fMRI co-activation patterns. Front Syst Neurosci. 2013; 7:101. [PubMed: 24550788]

Liu X, Duyn JH. Time-varying functional network information extracted from brief instances of spontaneous brain activity. Proc Natl Acad Sci U S A. 2013; 110:4392–4397. [PubMed: 23440216]

Manelis A, Ladouceur CD, Graur S, Monk K, Bonar LK, Hickey MB, Dwojak AC, Axelson D, Goldstein BI, Goldstein TR, Bebko G, Bertocci MA, Hafeman DM, Gill MK, Birmaher B, Phillips ML. Altered amygdala-prefrontal response to facial emotion in offspring of parents with bipolar disorder. Brain. 2015

Maren S. Is there savings for pavlovian fear conditioning after neurotoxic basolateral amygdala lesions in rats? Neurobiol Learn Mem. 2001; 76:268–283. [PubMed: 11726237]

McDonald AJ. Cortical pathways to the mammalian amygdala. Prog Neurobiol. 1998; 55:257–332. [PubMed: 9643556]

McDonald AJ, Mascagni F, Guo L. Projections of the medial and lateral prefrontal cortices to the amygdala: a Phaseolus vulgaris leucoagglutinin study in the rat. Neuroscience. 1996; 71:55–75. [PubMed: 8834392]

Mishra A, Rogers BP, Chen LM, Gore JC. Functional connectivity-based parcellation of amygdala using self-organized mapping: a data driven approach. Hum Brain Mapp. 2014; 35:1247–1260. [PubMed: 23418140]

Mosher CP, Zimmerman PE, Gothard KM. Response characteristics of basolateral and centromedial neurons in the primate amygdala. J Neurosci. 2010; 30:16197–16207. [PubMed: 21123566]

Mumford JA, Poline JB, Poldrack RA. Orthogonalization of regressors in FMRI models. PLoS One. 2015; 10:e0126255. [PubMed: 25919488]

Musil SY, Olson CR. Organization of cortical and subcortical projections to medial prefrontal cortex in the cat. J Comp Neurol. 1988; 272:219–241. [PubMed: 2456312]

Neubert FX, Mars RB, Thomas AG, Sallet J, Rushworth MF. Comparison of human ventral frontal cortex areas for cognitive control and language with areas in monkey frontal cortex. Neuron. 2014; 81:700–713. [PubMed: 24485097]

Ochsner KN, Bunge SA, Gross JJ, Gabrieli JD. Rethinking feelings: an FMRI study of the cognitive regulation of emotion. J Cogn Neurosci. 2002; 14:1215–1229. [PubMed: 12495527]

Ochsner KN, Gross JJ. The cognitive control of emotion. Trends Cogn Sci. 2005; 9:242–249. [PubMed: 15866151]

Öngur D, Price JL. The organization of networks within the orbital and medial prefrontal cortex of rats, monkeys and humans. Cereb Cortex. 2000; 10:206–219. [PubMed: 10731217]

Paré D, Collins DR. Neuronal correlates of fear in the lateral amygdala: multiple extracellular recordings in conscious cats. J Neurosci. 2000; 20:2701–2710. [PubMed: 10729351]

Petrides M, Pandya DN. Comparative cytoarchitectonic analysis of the human and the macaque ventrolateral prefrontal cortex and corticocortical connection patterns in the monkey. Eur J Neurosci. 2002; 16:291–310. [PubMed: 12169111]

Phan KL, Wager T, Taylor SF, Liberzon I. Functional neuroanatomy of emotion: a meta-analysis of emotion activation studies in PET and fMRI. Neuroimage. 2002; 16:331–348. [PubMed: 12030820]

Phelps EA, LeDoux JE. Contributions of the amygdala to emotion processing: from animal models to human behavior. Neuron. 2005; 48:175–187. [PubMed: 16242399]

Phillips ML, Ladouceur CD, Drevets WC. A neural model of voluntary and automatic emotion regulation: implications for understanding the pathophysiology and neurodevelopment of bipolar disorder. Mol Psychiatry. 2008; 13:833–857.

Phillips ML, Swartz HA. A critical appraisal of neuroimaging studies of bipolar disorder: toward a new conceptualization of underlying neural circuitry and a road map for future research. Am J Psychiatry. 2014; 171:829–843. [PubMed: 24626773]

Price, JL. Architectonic structure of the orbital and medial prefrontal cortex. In: Zald, DH., Rauch, SL., editors. Orbitofrontal cortex. Oxford University Press; Oxford: 2006.

Price, JL., Russchen, FT., Amaral, DG. II: The Amygdaloid Complex. New York: Elsevier Science; 1987. The Limbic Region.

Qin S, Young CB, Supekar K, Uddin LQ, Menon V. Immature integration and segregation of emotion-related brain circuitry in young children. Proc Natl Acad Sci U S A. 2012; 109:7941–7946. [PubMed: 22547826]

Ray RD, Zald DH. Anatomical insights into the interaction of emotion and cognition in the prefrontal cortex. Neurosci Biobehav Rev. 2012; 36:479–501. [PubMed: 21889953]

Reid AT, Hoffstaedter F, Gong G, Laird AR, Fox P, Evans AC, Amunts K, Eickhoff SB. A seed-based cross-modal comparison of brain connectivity measures. Brain Struct Funct. 2016

Roy AK, Shehzad Z, Margulies DS, Kelly AM, Uddin LQ, Gotimer K, Biswal BB, Castellanos FX, Milham MP. Functional connectivity of the human amygdala using resting state fMRI. Neuroimage. 2009; 45:614–626. [PubMed: 19110061]

Sah P, Faber ES, Lopez De Armentia M, Power J. The amygdaloid complex: anatomy and physiology. Physiol Rev. 2003; 83:803–834. [PubMed: 12843409]

Sander D, Grafman J, Zalla T. The human amygdala: an evolved system for relevance detection. Rev Neurosci. 2003; 14:303–316. [PubMed: 14640318]

Satterthwaite TD, Wolf DH, Loughead J, Ruparel K, Elliott MA, Hakonarson H, Gur RC, Gur RE. Impact of in-scanner head motion on multiple measures of functional connectivity: relevance for studies of neurodevelopment in youth. Neuroimage. 2012; 60:623–632. [PubMed: 22233733]

Seeley WW, Menon V, Schatzberg AF, Keller J, Glover GH, Kenna H, Reiss AL, Greicius MD. Dissociable intrinsic connectivity networks for salience processing and executive control. J Neurosci. 2007; 27:2349–2356. [PubMed: 17329432]

Solano-Castiella E, Schafer A, Reimer E, Turke E, Proger T, Lohmann G, Trampel R, Turner R. Parcellation of human amygdala in vivo using ultra high field structural MRI. Neuroimage. 2011; 58:741–748. [PubMed: 21726652]

Stefanacci L, Amaral DG. Some observations on cortical inputs to the macaque monkey amygdala: an anterograde tracing study. J Comp Neurol. 2002; 451:301–323. [PubMed: 12210126]

Turkeltaub PE, Eden GF, Jones KM, Zeffiro TA. Meta-analysis of the functional neuroanatomy of single-word reading: method and validation. Neuroimage. 2002; 16:765–780. [PubMed: 12169260]

Ubeda-Banon I, Novejarque A, Mohedano-Moriano A, Pro-Sistiaga P, de la Rosa-Prieto C, Insausti R, Martinez-Garcia F, Lanuza E, Martinez-Marcos A. Projections from the posterolateral olfactory amygdala to the ventral striatum: neural basis for reinforcing properties of chemical stimuli. BMC Neurosci. 2007; 8:103. [PubMed: 18047654]

van den Heuvel MP, Hulshoff Pol HE. Exploring the brain network: a review on resting-state fMRI functional connectivity. Eur Neuropsychopharmacol. 2010; 20:519–534. [PubMed: 20471808]

Vincent JL, Kahn I, Snyder AZ, Raichle ME, Buckner RL. Evidence for a frontoparietal control system revealed by intrinsic functional connectivity. J Neurophysiol. 2008; 100:3328–3342. [PubMed: 18799601]

Ye AQ, Zhan L, Conrin S, GadElKarim J, Zhang A, Yang S, Feusner JD, Kumar A, Ajilore O, Leow A. Measuring embeddedness: Hierarchical scale-dependent information exchange efficiency of the human brain connectome. Hum Brain Mapp. 2015; 36:3653–3665. [PubMed: 26096223]

Yeo BT, Krienen FM, Sepulcre J, Sabuncu MR, Lashkari D, Hollinshead M, Roffman JL, Smoller JW, Zollei L, Polimeni JR, Fischl B, Liu H, Buckner RL. The organization of the human cerebral cortex estimated by intrinsic functional connectivity. J Neurophysiol. 2011; 106:1125–1165. [PubMed: 21653723]

Yeo BT, Tandi J, Chee MW. Functional connectivity during rested wakefulness predicts vulnerability to sleep deprivation. Neuroimage. 2015; 111:147–158. [PubMed: 25700949]

Highlights

- We directly compare task-based and resting state patterns of amygdala connectivity
- Amygdala subregions show distinct connectivity patterns
- All amygdala subregions show connectivity with the right VLPFC
- The amygdala interacts with many large-scale neural networks

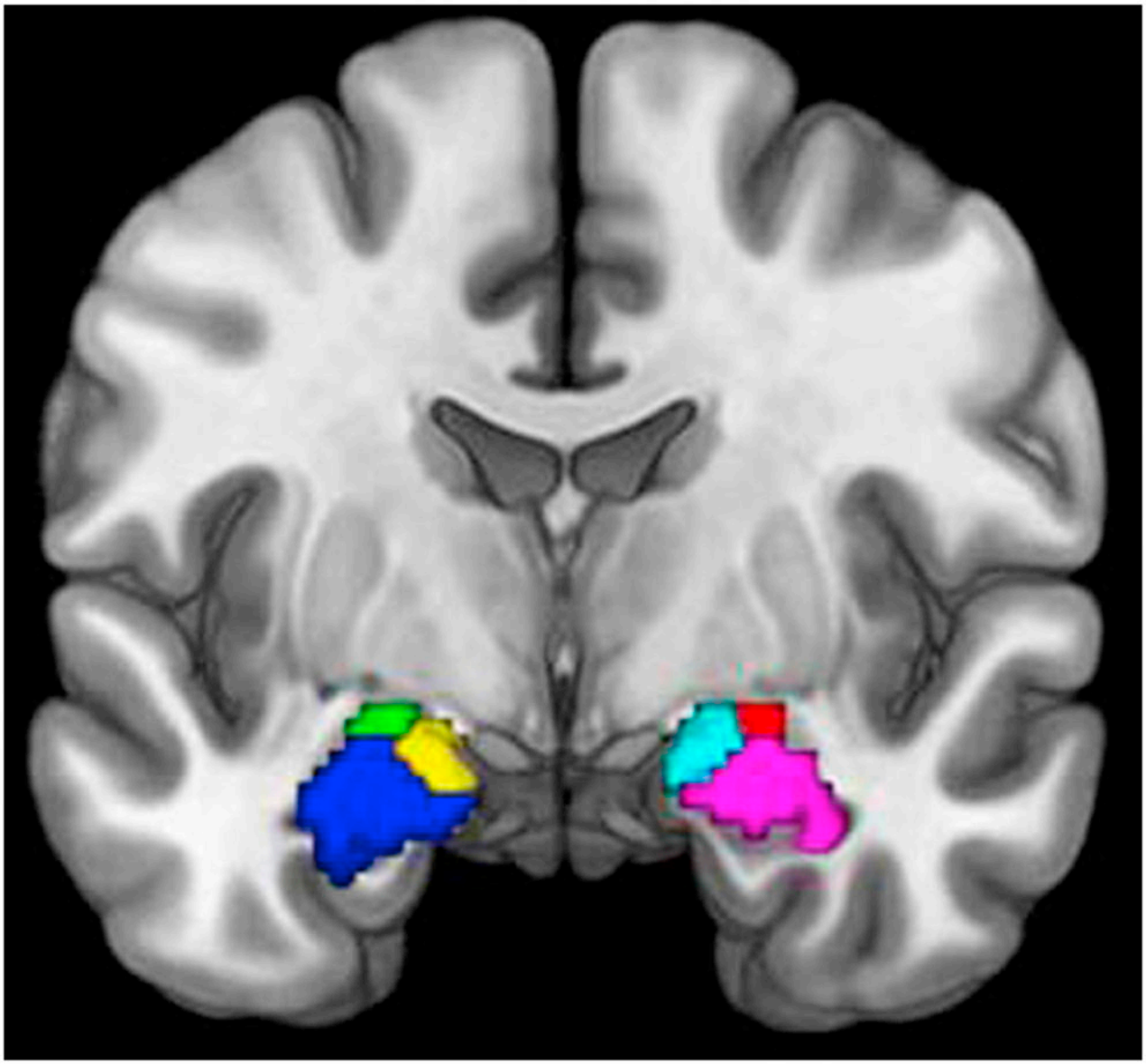

Fig. 1.

The amygdala seed regions: Green = Left centromedial (x= −22, y= −4, z= −16), Red = Right centromedial (x= 24, y= −12, z= −14), Blue = Left laterobasal (x= −26, y= −4, z= −34), Violet = Right laterobasal (x= 30, y= −2, z= −34), Yellow = Left superficial (x= −16, y= −10, z= −20), Cyan = Right superficial (x= 18, y= −6, z= −20). Seeds were created with the SPM Anatomy Toolbox, registered to MNI space and sampled to 2mm voxel resolution.

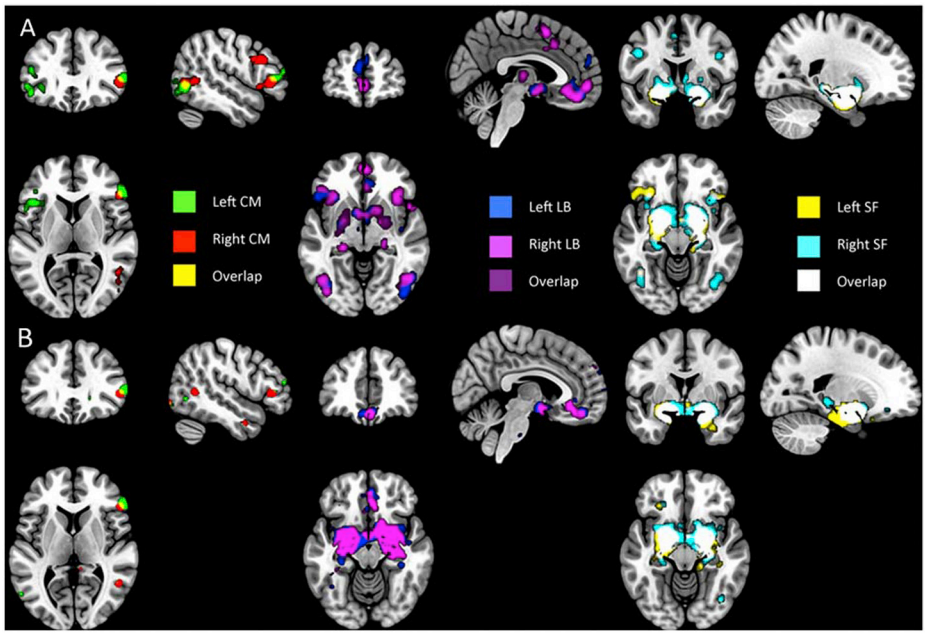

Fig. 2.

Meta-analytic connectivity modeling (MACM) of each of the centromedial, laterobasal and superficial amygdala subregions without (A) and with (B) base rate correction (SCALE). Results are shown at $p<.001$ with a $p<.05$ FWE cluster-wise correction. *Data obtained from BrainMap database.*

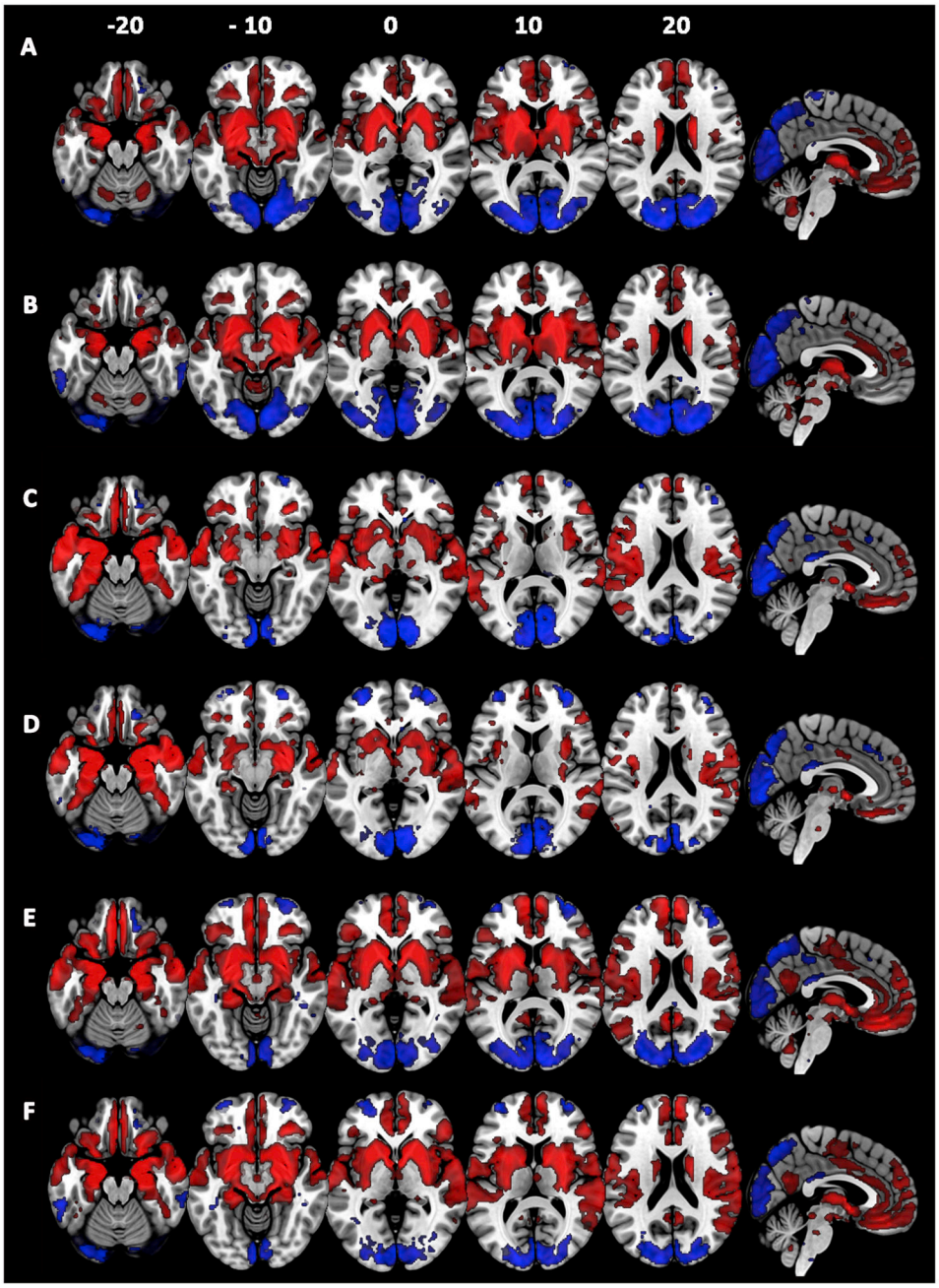

Fig. 3.

Rs-fmri connectivity of each of the centromedial (CM), laterobasal (LB) and superficial (SF) amygdala subregions. Red= regions positively correlated with each amygdala subregion. Blue= regions negatively correlated with each amygdala subregion. A = Left CM, B = Right CM, C = Left LB, D = Right LB, E = Left SF, F = Right SF. To highlight differences in amygdala subregion connectivity, results are shown at voxel-level $p<.05$ FWE corrected. *Data obtained from the NKI/Rockland rs-fmri dataset.*

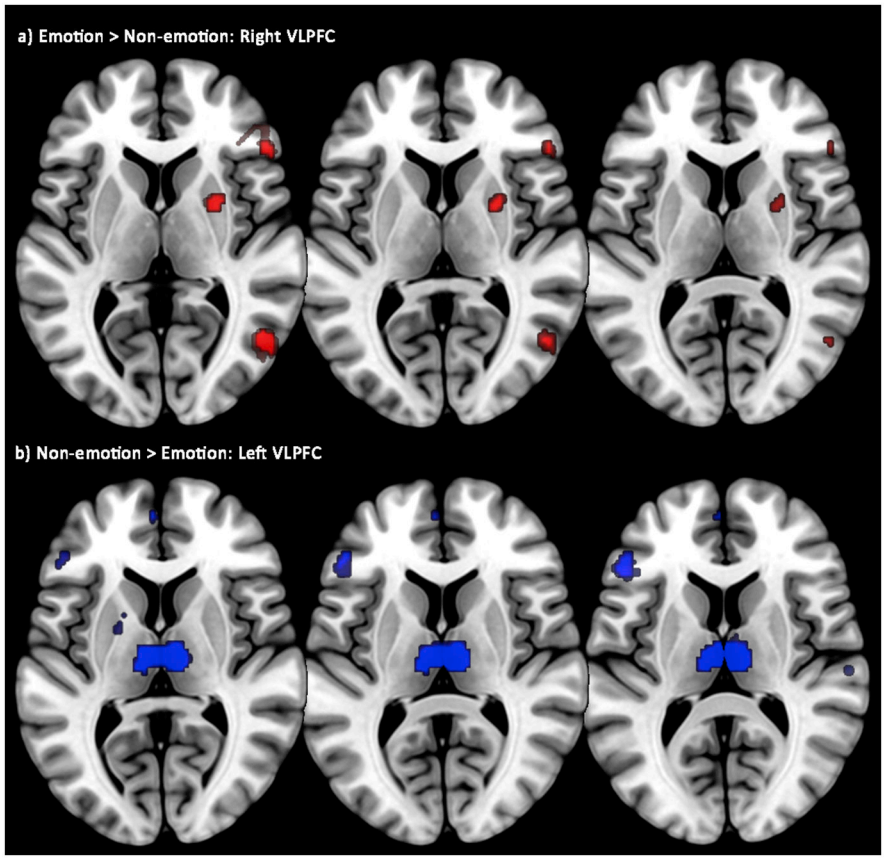

Fig. 4.

Contrast of emotion vs. non-emotion meta-analytic connectivity modeling (MACM) co-activation maps, illustrating a dissociation in co-activation between the right and left VLPFC for emotion (a) vs. non-emotion (b) studies. Results are shown at $p<.001$ with a $p<.05$ FWE cluster-wise correction. *Data obtained from BrainMap database.*

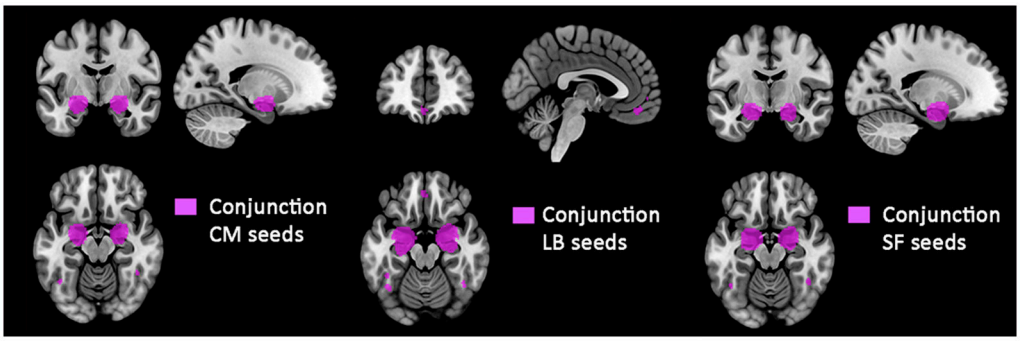

Fig. 5.

Meta-analytic connectivity modeling (MACM) maps illustrating areas of conjunction between emotion and non-emotion studies for each of the centromedial, laterobasal and superficial nuclei. Results are shown at $p<.001$ with a $p<.05$ FWE cluster-wise correction. *Data obtained from BrainMap database.*

Table 1

Regions showing co-activation with each of the amygdala subregions, from the MACM and SCALE analyses. “rs-fmri correlation” denotes the presence of a significant positive or negative correlation of low frequency BOLD of the corresponding amygdala subregion in a given MACM or SCALE cluster (‘convergent activation’). Cluster size, provided in parentheses, were significant at p<.05 FWE corrected (corrected for voxels within the mask rather than the whole brain). MACM contrast denotes the presence of a significant difference in the modeled activation scores in terms of contrasts (>: modeled activation in region A is greater than B) and conjunctions (=: regions A and B both coactivate the cluster).

								SCALE			
Amygdala sub-region	**Peak voxel (x, y, z)**	**Size (voxels)**	**z-score**	**rs-fmri correlation**	**T-statistic**	**MACM contrast**	**Peak voxel (x,y,z) if different**	**Size (voxels)**	**z-score**	**rsfmri correlation**	**T-statistic**
Left Centromedial (CM)											
Left amygdala (CM/LB/SF)	−22 −6 −14	1299	8.87	Positive (1132)	87.50	=Right CM (1027) =Left LB (1216) =Right LB (1203) =Left SF (1199) =Right SF (1037)	-	1255	8.50	Positive (1064)	87.5
Left hippocampus/parahippocampal gyrus				Positive (1132)		> Right CM (716) > Right SF (757)				Positive (1064)	
Right amygdala (CM/LB/SF)	24 −4 −14	1205	8.50	Positive (1019)	20.77	=Right CM (1090) =Left LB (1067) =Right LB (1156) =Left SF (1156) =Right SF (1112)	-	1205	8.31	Positive (951)	20.77
Right hippocampus/parahippocampal gyrus				Positive (1019)			36 −34 −16	62	8.15	None	
Right putamen				None							
Left fusiform gyrus	−42 −58 −18	775	6.95	Positive (66)		=Right CM (305) =Right LB (468) =Left SF (308) > Right SF (115) > Right CM (162)	-	250	8.19	None	
Left inferior occipital gyrus				Negative (199)	7.91	> Right CM (162) > Left SF (264) > Right SF (78)					
Left inferior frontal gyrus (pars triangularis)	−46 20 20	494	4.98	Positive (138)	6.69	=Right CM (82) =Left LB (353) > Right LB (191) > Left SF (142) > Right SF (66)					
Left insula						=Left RM (167) =Left SF (186) =Right SF (167)					
Right fusiform gyrus	42 −52 −20	364	7.32	None		=Right CM (166) =Right LB (196) =Left SF (152) =Right SF (253)	-	257	8.19	None	
Right inferior temporal gyrus						> Left SF (282)					
Right middle temporal gyrus	50 −66 −2	319	5.47	Negative (248)	6.92	=Right LB (192) =Left SF (111) =Right SF (122)					
Right inferior occipital gyrus				Negative (248)	6.18	> Right SF (44)					
Right inferior frontal gyrus (pars triangularis)	56 32 6	136	5.32	Positive (87)	7.74	=Right LB (63) =Left SF (102) > Right SF (83)	-	115	8.17	Positive (66)	7.27
Left inferior frontal gyrus (pars triangularis)	−50 22 −6	124	3.95	Positive (68)	5.23	> Right CM (24) > Right LB (74) =Left SF (108)					

			SCALE							
Amygdala sub-region	**Peak voxel (x, y, z)**	**Size (voxels)**	**z-score**	**rs-fmri correlation**	**T-statistic**	**MACM contrast**	**Peak voxel (x,y,z) if different**	**Size (voxels)**	**z-score**	**rsfmri correlation**	**T-statistic**
						> Right SF (27)					
							Left cerebellum (−6 −80 −38)	58	8.15	None	
Right Centromedial (CM)											
						=Left CM (1090)					
						=Left LB (1174)					
						=Right LB (1322)					
						=Left SF (1195)					
Right amygdala (CM/LB/SF)	24 −4 −14	1438	8.69	Positive (1279)	87.22	=Right SF (1207)	-	1392	8.41	Positive (1207)	87.22
						> Left CM (782)					
						>Right LB (633)					
						> Left SF (733)					
Right hippocampus/parahippocampal gyrus				Positive (1279)		> Right SF (617)					
						> Left CM (49)					
Right caudate nucleus				Positive (1279)		=Right LB (1322)					
						=Left LB (1090)					
						=Right LB (1095)					
Left amygdala (CM/LB/SF)	−22 −6 −14	1128	8.46	Positive (973)	19.42	=Left SF (1090)	-	1083	8.29	Positive (909)	19.42
						=Right SF (1002)					
Left hippocampus/parahippocampal gyrus						> Left CM (34)					
				Positive (973)		>Right LB (333)					
						=Left LB (302)					
						>Right LB (123)					
						=Right LB (255)					
Left fusiform gyrus	−42 −56 −20	338	5.38	None		=Left SF (195)					
						=Right SF (229)					
Left inferior occipital gyrus				Negative (77)	4.57						
						=Left LB (139)					
						>Right LB (124)					
						=Right LB (143)					
						=Left SF (127)					
Right fusiform gyrus	40 −48 −22	182	5.85	None		=Right SF (157)	-	94	8.17	None	
						> Left CM (103)					
						> Left LB (126)					
						>Right LB (62)					
						> Left SF (160)					
						> Right SF (85)					
Right inferior frontal gyrus ext into precentral gyrus	50 20 29	181	5.06	Positive (47)	4.87	=Right SF (68)					
						> Left CM (122)					
						> Left LB (129)					
						=Right LB (73)					
Right inferior frontal gyrus (pars triangularis)	50 30 4	154	5.19	Positive (97)	7.64	> Left SF (122)	-	71	8.17	Positive (66)	7.64
						=Right SF (88)					
						=Right LB (71)					
Left inferior frontal gyrus (pars opercularis)	−44 20 22	116	5.18	None		> Left SF (50)					
						=Right SF (73)					
						> Left LB (62)					
Right middle temporal gyrus	50 −64 2	110	4.33	None		>Right LB (63)					
						=Left SF (64)					
Left Laterobasal (LB)											
						=Left CM (1090)					
						=Right LB (3957)					
						=Left SF (1666)					
Left amygdala (CM/LB/SF)	−22 −6 −20	6041	9.11	Positive (4055)	69.03	=Right SF (2746)	-	7107	8.62	Positive (2570)	69.03
						> Left CM (1293)					
						> Right CM (1256)					
						> Right LB (1600)					
						> Left SF (1175)					
Left hippocampus/parahippocampal gyrus				Positive (4055)		> Right SF (1571)			8.39	Positive (2570)	

								SCALE			
Amygdala sub-region	**Peak voxel (x, y, z)**	**Size (voxels)**	**z-score**	**rs-fmri correlation**	**T-statistic**	**MACM contrast**	**Peak voxel (x,y,z) if different**	**Size (voxels)**	**z-score**	**rsfmri correlation**	**T-statistic**
Left caudate				Positive (4055)		> Right LB (32)				Positive (93)	10.41
Right caudate				Positive (4055)						None	
Right amygdala (CM/LB/SF)				Positive (4055)		=Left CM (1067) =Right LB (3957) =Left SF (1372)					
Right hippocampus/parahippocampal gyrus				Positive (4055)		> Left CM (491) =Right CM (1174) =Right LB (3957) > Left SF (337) > Right SF (410) =Right SF (2746)	-	50	8.16	Positive (41)	5.41
Left fusiform gyrus				Positive (4055)		=Left CM (699) =Right CM (302) > Right LB (271) =Left SF (313) =Right SF (428) > Right SF (76)	-	240	8.22	Positive (222)	8.80
Left inferior frontal gyrus (pars triangularis)	−44 30 8	962	6.04	Positive (480)	7.12	> Left CM (26) =Right CM (95) =Right LB (532) > Right LB (121) > Right SF (31)					
Left insula						=Left SF (504)					
Right fusiform gyrus	42 −54 −20	832	6.16	Positive (117)	7.10	=Right CM (139) =Right LB (446) =Left SF (129)	-	89	8.20	Positive (23)	5.98
Right middle temporal gyrus				None		> Right LB (50) =Left SF (131)	-	136	8.20	None	
Right inferior occipital gyrus				None		> Right LB (69) > Left SF (72) > Right SF (15)	-	57	8.19	None	
Right inferior temporal gyrus						> Left SF (52)					
Right frontal medial cortex, ventral	2 48 −16	347	5.71	Positive (70)	8.12	> Left CM (132) > Right CM (93) =Right LB (179) > Left SF (58) > Right SF (23)	-	237	8.20	Positive (67)	7.87
Left frontal medial cortex, dorsal	−4 56 14	198	5.01	Positive (112)	7.79	> Right LB (117) > Left SF (24) > Right SF (56)	-	229	8.19	Positive (91)	7.38
Left lateral occipital gyrus	−46 −72 22	190	5.92	Negative (111)	5.90	> Right LB (136) > Left SF (148) > Right SF (98)	-	207	8.20	Negative (98)	5.79
Right inferior frontal gyrus (pars triangularis)	52 32 6	180	5.02	Positive (167)	8.05	=Right LB (111) =Left SF (118)	-	107	8.19	Positive (88)	7.94
Left thalamus	−8 −12 2	149	4.9	None		=Left LB (113)					
							Right medial temporal pole (42 16 −38)	119	8.16	None	
							Right middle temporal gyrus (46 −70 22)	97	8.17	None	
							Left cerebellum (−6 −52 −42)	54	8.15	None	
Right Laterobasal (LB)											
Right hippocampus/parahippocampal gyrus	24, −4, −20	5129	9.07	Positive (3832)	62.69	> Left CM (1618) > Right CM (1159) > Left LB (2010) > Left SF (1506) =Left CM (1156)	-	6632	8.60	Positive (2771)	62.69

								SCALE			
Amygdala sub-region	**Peak voxel (x, y, z)**	**Size (voxels)**	**z-score**	**rs-fmri correlation**	**T-statistic**	**MACM contrast**	**Peak voxel (x,y,z) if different**	**Size (voxels)**	**z-score**	**rsfmri correlation**	**T-statistic**
Right amygdala (CM/LB/SF)				Positive (3832)		> Right SF (1297) =Right CM (1322) =Left LB (3957) =Left SF (1635) =Right SF (3074)					
Left amygdala (CM/LB/SF)				Positive (3832)		=Left CM (1203) =Right CM (1095) = Left LB (3957) =Left SF (1510)					
Right caudate nucleus				Positive (3832)		=Right CM (1322)					
Left hippocampus/parahippocampal gyrus				Positive (3832)		> Left CM (324) > Left SF (386) > Right SF (743)	-	155	8.18	Positive (106)	7.96
Left insula	−36 22 2	871	6.82	Positive (15)	6.17	=Left CM (167) =Left LB (532) > Left LB (74) =Left SF (382) =Right SF (305)					
Left precentral gyrus				None		> Left SF (15) =Right SF (155)					
Left inferior frontal gyrus				Positive (234)		=Left LB (532)					
Right inferior frontal gyrus (pars triangularis)	50 30 4	705	5.65	Positive (218)	7.12	=Right CM (73) =Left LB (111) =Left SF (79) =Right SF (98)	-	123	8.19	Positive (112)	7.12
Right fusiform gyrus	42 −46 −22	675	6.3	Positive (205)	8.25	=Left CM (196) =Right CM (143) =Left LB (446) =Left SF (108) =Right SF (420)	-	138	8.20	Positive (109)	8.25
Right inferior temporal gyrus				None		> Left SF (37)				Positive (109)	
Right middle temporal gyrus				None		=Left CM (192) =Left SF (98)	60 −10 −18	69	8.16	Positive (68)	9.48
Right inferior occipital gyrus				None		> Left LB (111)					
Left inferior temporal gyrus	−44 -66 −6	669	5.00	None		=Left CM (468) =Right CM (255) =Left LB (600) > Left SF (19)					
Left fusiform gyrus				Positive (218)	8.05	=Left SF (189) =Right SF (323) > Right SF (31)					
Left inferior occipital gyrus				None							
Frontal medial cortex, ventral	0 44 −18	639	6.02	Positive (53)	6.33	>Right CM (291) =Left LB (179) > Left SF (94) > Right SF (304)	-	332	8.20	Positive (31)	5.83
Left mid orbital gyrus				None		> Left CM (231) > Left LB (83)					
Right mid orbital gyrus				None		> Left CM (122) > Left SF (129) > Right SF (304)	4 54 −10	63	3.35	None	
Left superior medial gyrus	−2 20 42	453	5.68	None		> Left LB (126) =Right SF (80)	−10 54 32	94	8.17	Positive (39)	6.44
Right posterior medial gyrus						> Left LB (41) > Left SF (32)					

		SCALE								
Amygdala sub-region	**Peak voxel (x, y, z)**	**Size (voxels)**	**z-score**	**rs-fmri correlation**	**T-statistic**	**MACM contrast**	**Peak voxel (x,y,z) if different**	**Size (voxels)**	**z-score**	**rsfmri correlation**	**T-statistic**
						=Right SF (60)					
Left thalamus	−10 −14 4	330	5.71	None		=Left LB (113)					
Right thalamus				Positive (70)	6.33	=Right SF (106)					
						=Right CM (103)					
						> Left SF (31)					
Right precentral gyrus ext into inferior frontal gyrus	48 8 28	184	5.2	None		=Right SF (79)					
Left Superficial (SF)											
						=Left CM (1199)					
						=Right CM (1090)					
						=Left LB (1666)					
						=Right LB (1510)					
Left amygdala (CM/LB/SF)	−20 −4 −16	1896	8.97	Positive (1483)	66.23	=Right SF (1370)	-	2050	8.55	Positive (1426)	66.23
						> Left CM (824)					
						> Right CM (871)					
						> Right LB (1046)					
Left hippocampus/parahippocampal gyrus				Positive (1483)		> Right SF (1086)					
Left caudate				Positive (1483)		=Right SF (1370)					
Left putamen						> Left LB (899)					
						=Left CM (1156)					
						=Right CM (1195)					
						=Left LB (1372)					
Right amygdala (CM/LB/SF)	22 −4 −16	1797	8.52	Positive (1387)	23.05	=Right LB (1635)	-	2108	8.32	Positive (1400)	23.05
						=Right SF (1554)					
						> Left CM (589)					
						> Left LB (819)					
Right hippocampus/parahippocampal gyrus				Positive (1387)		> Right SF (33)	38 −32 −14		8.15	Positive (23)	13.09
						> Right CM (152)					
						> Left LB (43)					
						> Right LB (186)					
Left inferior frontal gyrus (pars opercularis) ext into pars triangularis	−44 26 2	724	4.98	Positive (510)	13.11	>Right SF (163)					
						=Left CM (186)					
						=Left LB (504)					
						=Right LB (382)					
Left insula				Positive (23)		=Right SF (203)					
						=Left CM (308)					
						=Right CM (195)					
						=Left LB (313)					
						=Right LB (189)					
Left fusiform gyrus	−42 −56 −18	335	6.40	Positive (168)	7.30	=Right SF (240)					
Left inferior temporal gyrus				Positive (168)		> Right LB (35)	-	69	8.16	Positive (44)	6.11
						=Left CM (111)					
						=Right CM (84)					
						=Left LB (131)					
						=Right LB (98)					
Right middle temporal gyrus	50 −64 0	203	5.23	None		=Right SF (53)	−52 −64 0	68	8.17	None	
						> Right CM (132)					
						> Left LB (142)					
Right inferior frontal gyrus (pars orbitalis)	48 24 −12	187	4.31	None		> Right LB (40)					
Right temporal pole											
						=Left CM (102)					
						=Left LB (118)					
Right inferior frontal gyrus (pars triangularis)	54 32 6	167	4.68	Positive (116)	8.57	=Right LB (79)	-	75	8.17	Positive (60)	8.3
						=Left CM (152)					
						=Right CM (127)					
						=Left LB (129)					
						=Right LB (108)					
Right fusiform gyrus	40 −50 −22	152	5.95	Positive (65)	5.43	=Right SF (143)					

							SCALE			
Amygdala sub-region	**Peak voxel (x, y, z)**	**Size (voxels)**	**z-score**	**rs-fmri correlation**	**T-statistic**	**MACM contrast**	**Peak voxel (x,yz) if different**	**Size (voxels)**	**z-score**	**rsfmri correlation**	**T-statistic**
							Left superior medial gyrus (−2 62 22)	198	8.16	Positive (27)	11.94
							Left superior frontal gyrus (−12 42 52)	56	8.15	Positive (25)	9.56
							Left superior frontal gyrus (−14 56 32)	52	8.15	Positive (29)	10.21
Right Superficial (SF)											
						=Left CM (1112)					
						=Right CM (1207)					
						=Right LB (3074)					
Right amygdala (CM/LB/SF)	20 −4 −16	5061	8.84	Positive (3505)	86.27	=Left SF (1554)	-	3703	8.48	Positive (2580)	86.27
						=Left CM (1037)					
						=Left SF (1370)					
Left amygdala (CM/LB/SF)				Positive (3505)		=Right CM (1002)			8.33	Positive (2580)	
						> Left CM (109)					
						> Right CM (40)					
Left hippocampus/parahippocampal gyrus				Positive (3505)		> Left LB (29)			8.18	Positive (2580)	
Right caudate				Positive (3505)							
						> Left SF (331)					
						> Right CM (145)					
						> Left LB (1064)					
						> Right LB (2382)					
Left putamen ext into nucleus accumbens				Positive (3505)		> Left SF (1163)			8.18	Positive (2580)	
						> Left CM (1074)					
						> Right CM (661)					
Right hippocampus/parahippocampal gyrus				Positive (3505)		=Right LB (3074)			8.18	Positive (2580)	
Left thalamus				Positive (3505)							
						> Left SF (331)					
						> Left CM (57)					
						> Left LB (602)					
Right thalamus				Positive (3505)		=Right LB (106)					
						=Left CM (167)					
						=Right LB (305)					
						> Right LB (65)					
						=Left SF (203)					
Left insula				Positive (56)		> Left SF (146)					
						=Left CM (253)					
						=Right CM (157)					
						=Right LB (420)					
						> Right LB (110)					
Right fusiform gyrus	40 −50 −22	541	6.74	Positive (81)	7.23	=Left SF (143)	-	115	8.19	Positive (43)	7.19
Right inferior occipital cortex				None		> Left LB (72)					
						=Left CM (122)					
Right middle temporal gyrus				None		> Left SF (132)					
						=Left CM (391)					
						=Right CM (229)					
						=Left LB (428)					
						=Right LB (323)					
Left fusiform gyrus	−40 −58 −16	467	5.87	None		=Left SF (240)					
Left Inferior occipital gyrus				None		=Left LB (428)					
						> Right CM (80)					
						> Left LB (70)					
						=Right LB (239)					
						> Right LB (46)					
Right insula ext into Inferior frontal gyrus (pars opercularis)	36 20 −8	277	4.64	Positive (91)	6.16	> Left SF (46)					
						> Left CM (23)					
						=Left CM (76)					
						=Right CM (73)					
						> Left LB (41)					
						=Right LB (155)					
						> Right LB (85)					
Left inferior frontal gyrus (pars opercularis)	−44 18 24	240	5.74	None		> Left SF (66)					

							SCALE			
Amygdala sub-region	**Peak voxel (*x, y, z*)**	**Size (voxels)**	***z*-score**	**rs-fmri correlation**	**T-statistic**	**MACM contrast**	**Peak voxel (*x,y,z*) if different**	**Size (voxels)**	***z*-score**	**rsfmri correlation**	**T-statistic**
						> Left SF (27)					
						> Left LB (127)					
						=Right LB (60)					
Right superior frontal gyrus	2 10 54	236	4.65	Positive (15)	5.69	> Right LB (35)					
						> Left SF (128)					
Left superior frontal gyrus						=Right LB (80)					
						> Left CM (43)					
						=Right CM (88)					
						> Left LB (53)					
						=Right LB (98)					
Right inferior frontal gyrus (pars triangularis)	50 30 4	119	5.63	Positive (119)	10.35	> Left SF (33)	-	71	8.18	Positive (71)	10.35
						=Right CM (68)					
						> Left LB (41)					
						=Right LB (79)					
Right precentral gyrus	46 8 30	110	4.64	Positive (39)	6.81	> Left SF (69)					